DOI: 10.19884/j.1672-5220.202408005

Structural Reliability Analysis Method Based on Kriging and Spherical Cap Area Integral

ZHANG Jixiang[1], CHEN Zhenzhong[1*], CHEN Ge[1*], LI Xiaoke[2], ZHAO Pengcheng[3], PAN Qianghua[4]
1. College of Mechanical Engineering, Donghua University, Shanghai 201620, China
2. College of Mechanical and Electrical Engineering, Zhengzhou University of Light Industry, Zhengzhou 450002, China
3. Shanghai Technology and Innovation Vocational College, Shanghai 201620, China
4. China Special Equipment Inspection and Research Institute, Beijing 100029, China

Abstract: In the structural reliability analysis, the first-order reliability method (FORM) often yields significant errors when addressing nonlinear problems. Although the second-order reliability method (SORM) can provide higher accuracy, the additional computation of the Hessian matrix leads to lower computational efficiency. Additionally, when the dimensionality of the random variables is high, the approximation formula of SORM can result in larger errors. To address these issues, a structural reliability analysis method based on Kriging and spherical cap area integral is proposed. Firstly, this method integrates FORM with the quasi-Newton algorithm Broyden-Fletcher-Goldfarb-Shanno (BFGS), trains the Kriging model by using sample points from the algorithm's iteration process, and combines the Kriging model with gradient information to approximate the Hessian matrix. Then, the failure surface is approximated as a rotating paraboloid, utilizing the spherical cap to replace the complex surface. For the *n*-dimensional case, the hyperspherical cap area expression is combined with the integral method to calculate the failure probability. Finally, the method is validated through three examples, demonstrating improved computational accuracy and efficiency compared to traditional methods.

Keywords: structural reliability analysis; quasi-Newton algorithm; Kriging model; spherical cap area integral
CLC number: TH122; TB114.3 **Document code**: A
Article ID: 1672-5220(2025)04-0409-08

Open Science Identity (OSID)

0 Introduction

In the design and application of engineering structures, uncertainty factors such as material properties, applied loads and geometric parameters can significantly affect structural performance[1]. The purpose of the reliability analysis is to account for these uncertain factors as random variables and to calculate the probability of structural failure based on their distributions[2]. Therefore, research on reliability analysis methods is crucial for evaluating the performance of structures and enhancing their safety and long-term stability.

Reliability analysis methods primarily include simulation methods and approximate analytical methods. Among these, Monte Carlo simulation (MCS)[3] is the most used simulation method. MCS calculates the response values of structures by generating samples from the actual probability distribution, and then the failure probability at the design point is accurately derived from the number of failed sample points. Despite its accuracy, MCS requires many sample points, leading to significant computational costs. To address the computational inefficiency of MCS, several improved methods have been developed, such as the subset simulation (SS) method[4], the importance sampling (IS) method[5] and the adaptive sequential sampling method[6]. With the development of these improved methods, some surrogate modeling techniques, such as the Kriging method[7], have been widely applied in the reliability analysis due to their strong ability to approximate nonlinear models, as well as their efficient spatial modeling and prediction capabilities.

The first-order reliability method (FORM) and the second-order reliability method (SORM) are the most prevalent in the approximate analytical methods[8]. FORM involves a first-order Taylor expansion of the limit-state function (LSF) at the most probable point of failure (MPP). The key to FORM is identifying the MPP to determine the first-order reliability index β. The Hasofer-Lind-Rackwitz-Fiessler (HLRF) method[9-10] is the most frequently used approach for locating the MPP. While effective for simpler LSFs, it exhibits poor convergence and low efficiency when dealing with complex LSFs. Consequently, several improved HLRF

Received date: 2024-08-26
Foundation items: National Natural Science Foundation of China (No. 52375236); Fundamental Research Funds for the Central Universities, China (No. 23D110316)
* Correspondence should be addressed to CHEN Zhenzhong, email: zhenzh.chen@dhu.edu.cn; CHEN Ge, email: chenge@dhu.edu.cn
Citation: ZHANG J X, CHEN Z Z, CHEN G, et al. Structural reliability analysis method based on Kriging and spherical cap area integral [J]. *Journal of Donghua University (English Edition)*, 2025, 42(4): 409-416.

methods have been developed, such as the hybrid relaxed HLRF method[11], the improved chaotic control-based HLRF method[12] and the HLRF-BFGS method[13]. The HLRF-BFGS method combines the quasi-Newton BFGS algorithm with the HLRF method. Each iteration requires only the value of the objective function and the gradient, incorporating curvature information of the LSF, which significantly improves the convergence and efficiency of FORM.

SORM involves a second-order Taylor expansion of the LSF, determining the curvature at the MPP by using the Hessian matrix, and subsequently calculating the failure probability. Research on SORM has primarily focused on improving computational efficiency and accuracy. To improve the efficiency of SORM, Zhang et al.[14] proposed an SORM with first-order efficiency. Zeng et al.[15] introduced a reliability analysis method that used quasi-Newton algorithm to approximate the Hessian matrix. These methods improve the computational efficiency of SORM, but the accuracy is insufficient when dealing with problems with high levels of nonlinearity and dimensionality. To enhance the accuracy of SORM, Chen et al.[16-17] proposed a method for second-order parabolic approximation and further improved it by developing a reliability analysis method for calculating the division of the region where the approximated paraboloid intersects with the hyperspherical cap. Although this method improves the computational accuracy of SORM, it also increases the computational workload.

Considering the limitations of traditional reliability analysis methods mentioned above, to improve both the efficiency and accuracy of failure probability calculation, a structural reliability analysis method based on Kriging and spherical cap area integral is proposed. By constructing a Kriging model and incorporating gradient information from design points to approximate the Hessian matrix, the computational workload is reduced. Additionally, the failure probability is determined by using the hyperspherical cap area integral method to enhance computational accuracy. Finally, the feasibility of the proposed method is validated through three examples.

1 Review of Reliability Analysis Methods

Based on the distribution of the structural random variables, the failure probability P_f of the structure is obtained as[18]

$$P_f = \iint\cdots\int_{g(\boldsymbol{X})\leqslant 0} f(\boldsymbol{X})\,\mathrm{d}\boldsymbol{X}, \tag{1}$$

where $g(\boldsymbol{X})$ denotes the LSF; $\boldsymbol{X} = [X_1, X_2, \cdots, X_n]^{\mathrm{T}}$ represents the n-dimensional random vector.

In the reliability analysis, FORM especially excels in dealing with linear problems and can provide accurate results. When FORM is utilized to compute Eq. (1), the n-dimensional random vector $\boldsymbol{X}$ can be converted to an independent standard normal vector $\boldsymbol{U} = [U_1, U_2, \cdots, U_n]^{\mathrm{T}}$ by Rosenblatt transform[19], and then the LSF can be expressed by the first-order Taylor expansion at MPP as

$$g(\boldsymbol{X}) = g(\mathrm{RN}^{-1}(\boldsymbol{U})) = h(\boldsymbol{U}) = (\boldsymbol{U} - U_{\mathrm{MPP}})\nabla h(U_{\mathrm{MPP}}), \tag{2}$$

where RN denotes the function of Rosenblatt transformation; U_{MPP} is the final obtained design point; $\nabla h(U_{\mathrm{MPP}})$ denotes the gradient vector of LSF at MPP. FORM aims to search for the point with the shortest distance from the coordinate origin, i.e., the MPP. The distance between the coordinate origin and the MPP is called the reliability index β. The reliability problem can be converted into a constrained optimization problem:

$$\begin{aligned} &\min\ \beta = \frac{1}{2}\boldsymbol{U}^{\mathrm{T}}\boldsymbol{U}, \\ &\text{s.t.}\ \ h(\boldsymbol{U}) = 0. \end{aligned} \tag{3}$$

Subsequently, for FORM, the failure probability can be obtained as

$$P_{f,\,\mathrm{FORM}} = \Phi(-\beta). \tag{4}$$

When the degree of nonlinearity of the LSF is high, the result of FORM produces a large error, while SORM performs the second-order Taylor expansion of the LSF and accounts for the effect of curvature. The LSF is expressed as

$$h(\boldsymbol{U}) \approx h(U_{\mathrm{MPP}}) + (\boldsymbol{U} - U_{\mathrm{MPP}})^{\mathrm{T}}\nabla h(U_{\mathrm{MPP}}) + \frac{1}{2}(\boldsymbol{U} - U_{\mathrm{MPP}})^{\mathrm{T}}\nabla^2 h(U_{\mathrm{MPP}})(\boldsymbol{U} - U_{\mathrm{MPP}}), \tag{5}$$

where $\nabla^2 h(U_{\mathrm{MPP}})$ indicates the Hessian matrix. Taking the two-dimensional case as an example, as shown in Fig. 1, SORM approximates the LSF as a parabola, and the curvature K_i of the parabola at the MPP is determined by the Hessian matrix.

$$K_i = \frac{\boldsymbol{M}^{\mathrm{T}}\nabla^2 h(U_{\mathrm{MPP}})\boldsymbol{M}}{\nabla h(U_{\mathrm{MPP}})}, \tag{6}$$

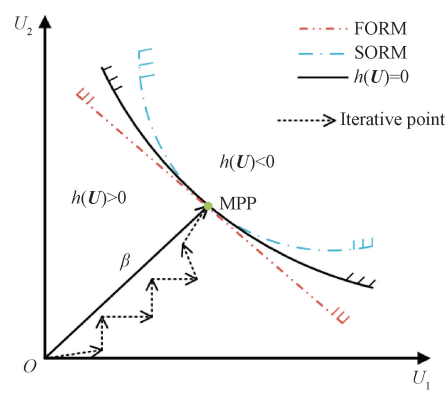

Fig. 1 Schematic view of FORM and SORM

where $\boldsymbol{M} = [U_1, U_2, \cdots, U_{n-1}, \alpha]^{\mathrm{T}}$ is the $n \times n$ orthogonal matrix by Gram-Schmidt orthogonalization and rotation, and the nth column $\alpha = -\nabla h(U_{\mathrm{MPP}})/$

$\| \nabla h(U_{\mathrm{MPP}}) \|$. Assume that a_i ($i=1, 2, \cdots, n$) is the parabolic coefficient, then $a_i = -K_i/2$, and thus the approximate parabolic function can be expressed as

$$Y(\boldsymbol{U}) = \beta + \sum_{i=1}^{n} a_i U_i^2 - U_n. \tag{7}$$

Subsequently, the failure probability is derived[20]:

$$P_{\mathrm{f,\ SORM}} = \Phi(-\beta) \prod_{i=1}^{n-1} (1 - \beta K_i)^{-1/2}. \tag{8}$$

For Eq. (8), although this method is more accurate than FORM, its approximation formula produces singular solutions, leading to large errors when $1 - \beta K_i < 0$, and solving the Hessian matrix brings additional computations[21]. Therefore, an improved method is proposed in the following sections.

2 Proposed Method

2.1 HLRF-BFGS method to solve FORM

To enhance the convergence and efficiency of FORM, this study combines HLRF with the quasi-Newton algorithm BFGS. The constrained optimization problem of Eq. (3) is transformed into an unconstrained optimization problem by introducing the Lagrange multiplier $\boldsymbol{\lambda}$:

$$\min\ l(\boldsymbol{U}, \boldsymbol{\lambda}) = \frac{1}{2}\boldsymbol{U}^{\mathrm{T}}\boldsymbol{U} + \boldsymbol{\lambda}^{\mathrm{T}} h(\boldsymbol{U}). \tag{9}$$

The new iteration point can be derived from the recursive equation:

$$U_k = d_k + U_{k-1}, \tag{10}$$

where U_k represents the design point in the standard normal space at the kth iteration, updated recursively from the previous point U_{k-1}; d_k denotes the step size of the kth iteration, with its update formula given by

$$d_k = \frac{[\nabla h(U_k)^{\mathrm{T}} \boldsymbol{B}_k U_k - h(U_k)]\boldsymbol{B}_k \nabla h(U_k)}{\nabla h(U_k)^{\mathrm{T}} \boldsymbol{B}_k \nabla h(U_k)} - \boldsymbol{B}_k U_k. \tag{11}$$

The inverse matrix $\boldsymbol{B}_k$ of the Hessian matrix can be obtained by using the update formula:

$$\boldsymbol{B}_{k+1} = \boldsymbol{B}_k + \left(1 + \frac{\boldsymbol{q}_k^{\mathrm{T}} \boldsymbol{B}_k \boldsymbol{q}_k}{\boldsymbol{p}_k^{\mathrm{T}} \boldsymbol{q}_k}\right)\left(\frac{\boldsymbol{p}_k \boldsymbol{p}_k^{\mathrm{T}}}{\boldsymbol{p}_k^{\mathrm{T}} \boldsymbol{q}_k}\right) - \frac{\boldsymbol{p}_k \boldsymbol{q}_k^{\mathrm{T}} \boldsymbol{B}_k + \boldsymbol{B}_k \boldsymbol{q}_k \boldsymbol{p}_k^{\mathrm{T}}}{\boldsymbol{p}_k^{\mathrm{T}} \boldsymbol{q}_k}, \tag{12}$$

where

$$\boldsymbol{q}_k = \nabla_x l(U_{k+1}, \lambda_{k+1}) - \nabla_x l(U_k, \lambda_k), \tag{13}$$

$$\boldsymbol{p}_k = h(U_{k+1}) - h(U_k), \tag{14}$$

$$\lambda_k = \frac{h(U_k) - \nabla h(U_k)^{\mathrm{T}} \boldsymbol{B}_k U_k}{\nabla h(U_k)^{\mathrm{T}} \boldsymbol{B}_k \nabla h(U_k)}. \tag{15}$$

Continue the algorithm's execution of the sequence until the specified termination criteria are satisfied:

$$|h(U_k)| < \eta \text{ and } 1 - \frac{|\nabla h(U_k)^{\mathrm{T}} U_k|}{\| \nabla h(U_k) \| \cdot \| U_k \|} < \eta \quad (\eta = 10^{-6} - 10^{-8}). \tag{16}$$

Through the above process, the design point U_{MPP} and the first-order reliability index β can be finally obtained.

2.2 Approximating Hessian matrix by Kriging model

The Kriging model is constructed by using the design points obtained from the iterative process of the HLRF-BFGS method, along with additional points selected by the center composite method at the final design point U_{MPP}. These points are used as sample points, denoted as $\underline{\boldsymbol{U}} = [\underline{U}_1, \underline{U}_2, \cdots, \underline{U}_m]$ (where m is the total number of sample points), with their corresponding function values $h(\underline{\boldsymbol{U}})$. In this framework, the construction of the Kriging model is divided into a regression model and a stochastic process:

$$\hat{h}(\boldsymbol{U}) = f^{\mathrm{T}}(\boldsymbol{U})\boldsymbol{P} + z(\boldsymbol{U}), \tag{17}$$

where $\hat{h}(\boldsymbol{U})$ is the predicted response value; $f(\boldsymbol{U})$ is the polynomial basis function of the vector; $\boldsymbol{P}$ is the vector of regression coefficients; $z(\boldsymbol{U})$ is a zero-mean Gaussian process with variance σ^2 and covariance:

$$\mathrm{Cov}[z(\underline{U}_c), z(\underline{U}_j)] = \sigma^2 \boldsymbol{R}(\theta, \underline{U}_c, \underline{U}_j), \tag{18}$$

where $c, j = 1, 2, \cdots, m$; $\boldsymbol{R}(\theta, \underline{U}_c, \underline{U}_j)$ is the correlation matrix of the sample training points; θ denotes the correlation parameter that determines the correlation matrix $\boldsymbol{R}$, given by the Gaussian correlation function:

$$\boldsymbol{R}(\theta, \underline{U}_c, \underline{U}_j) = \exp\left[\sum_{t=1}^{m} -\theta^{(t)} (\underline{U}_c^{(t)}, \underline{U}_j^{(t)})^2\right]. \tag{19}$$

Accordingly, the vector of regression coefficients $\boldsymbol{P}$ and the variance $\tilde{\boldsymbol{s}}(\boldsymbol{u})$ at any point can be expressed as

$$\boldsymbol{P} = (\boldsymbol{F}\boldsymbol{R}^{-1}\boldsymbol{F})\boldsymbol{F}\boldsymbol{R}^{-1} h(\underline{\boldsymbol{U}}), \tag{20}$$

$$\tilde{\boldsymbol{s}}(\boldsymbol{u}) = \sigma^2 \left[1 - \boldsymbol{v}^{\mathrm{T}}\boldsymbol{R}^{-1}\boldsymbol{v} + \frac{(1 - \boldsymbol{F}\boldsymbol{R}^{-1}\boldsymbol{v})^2}{\boldsymbol{F}^{\mathrm{T}}\boldsymbol{R}^{-1}\boldsymbol{F}}\right], \tag{21}$$

where $\boldsymbol{F}$ is an $m \times n$ matrix; $\boldsymbol{v}$ is the column vector of correlations between each training point and the prediction point.

Then, Eq. (17) can be converted:

$$\hat{h}(\boldsymbol{U}) = f^{\mathrm{T}}(\boldsymbol{U})\boldsymbol{P} + \boldsymbol{v}(\boldsymbol{U})^{\mathrm{T}} \boldsymbol{v}^*, \tag{22}$$

where $\boldsymbol{v}(\boldsymbol{U})^{\mathrm{T}} = [\boldsymbol{R}(\theta, \underline{U}_1, \boldsymbol{U}), \boldsymbol{R}(\theta, \underline{U}_2, \boldsymbol{U}), \cdots, \boldsymbol{R}(\theta, \underline{U}_m, \boldsymbol{U})]$ denotes the correlation function between any input vector and the sample points; $\boldsymbol{v}^*$ denotes the solution of $(h(\underline{\boldsymbol{U}}) - \boldsymbol{F}\boldsymbol{P})/\boldsymbol{R}$.

After constructing the Kriging model by the above method, the Kriging model is utilized to obtain the partial derivative information of the predicted points. Then, the Hessian matrix can be obtained by the finite difference method.

2.3 Hyperspherical cap area integral method

In the U-space, the MPP and β corresponding to the LSF can be obtained by FORM. For a two-dimensional reliability problem, assume that a circle is drawn with β as the radius, and the graph with the same probability density function value is a circle with a radius of ρ [16]. Then the β-circle is tangent to the LSF at the MPP, and the approximate parabola of the LSF at the MPP is obtained by solving the curvature outside the tangent point, thus dividing the whole area into failure area and safety area. Then, the proportion of the failure area between the β-circle and the ρ-circle is obtained as φ/π based on the ratio of the arc length of the circle, and then the failure probability is obtained as

$$P_{\mathrm{f}} = \int_{\beta}^{+\infty} \frac{\varphi}{\pi} \rho \exp\left(-\frac{\rho^2}{2}\right) \mathrm{d}\rho, \tag{23}$$

where (ρ, φ) is the standard normal variable (U_1, U_2) obtained by polar coordinate transformation:

$$\begin{cases} U_1 = \rho\cos(\varphi), \\ U_2 = \rho\sin(\varphi). \end{cases} \tag{24}$$

The expression between the angle φ_i and the approximate parabolic coefficient a_i is derived as

$$\varphi_i = \arccos\left(\frac{\sqrt{1 + 4a_i\beta + 4a_i^2\rho^2} - 1}{2a_i\rho}\right). \tag{25}$$

Further for n-dimensional problems ($n > 2$), the corresponding geometry is an n-dimensional hypersphere with the expression:

$$\rho^2 = U_1^2 + U_2^2 + \cdots + U_n^2. \tag{26}$$

The failure probability can be approximated as the proportion of the region where the paraboloid intersects the hypersphere to the ρ-sphere (excluding the β-sphere) [17]. The intersection region is an irregular elliptical arch, which is challenging to calculate directly. To simplify this, the failure surface is approximated by a rotating paraboloid. The intersection region between this rotating paraboloid and the spherical surface is approximated as a spherical cap, and the area of the spherical cap is used to approximate the area of the actual intersection region instead. The approximated rotating paraboloid can be derived from Eq. (7), and the area of the hyperspherical cap S in the n-dimensional case can be expressed as

$$S = \int_{D}\cdots\int \frac{\rho}{\sqrt{\rho^2 - (U_1^2 + U_2^2 + \cdots + U_n^2)}} \mathrm{d}U_1 \mathrm{d}U_2 \cdots \mathrm{d}U_n, \tag{27}$$

where the integration region $D = U_1^2 + U_2^2 + \cdots + U_n^2 \leqslant t^2$ is the projection of the hyperspherical cap in the horizontal plane projection, and t is the short radius of the projected figure.

After coordinate transformation and mathematical processing, according to Ref. [17], Eq. (27) can be further converted.

$$\text{When } n \text{ is odd, } S = \left\{1 - \frac{\sqrt{\rho^2 - r_i^2}}{\rho}\left[1 + \sum_{k=1}^{(n-3)/2} \frac{(2k-1)!!}{(2k)!!}\left(\frac{r_i}{\rho}\right)^{2k}\right]\right\} \frac{2\pi^{\frac{(n-1)}{2}}\rho^{(n-1)}}{\Gamma\left(\frac{n-1}{2}\right)} \frac{(n-3)!!}{(n-2)!!}, \tag{28}$$

$$\text{when } n \text{ is even, } S = \left\{\arcsin\frac{r_i}{\rho} - \frac{\sqrt{\rho^2 - r_i^2}}{\rho}\left[1 + \sum_{k=1}^{(n-2)/2} \frac{(2k-2)!!}{(2k-1)!!}\left(\frac{r_i}{\rho}\right)^{2k-1}\right]\right\} \frac{2\pi^{\frac{(n-1)}{2}}\rho^{(n-1)}}{\Gamma\left(\frac{n-1}{2}\right)} \frac{(n-3)!!}{(n-2)!!}, \tag{29}$$

where the radius of the hypersphere cap can be obtained from the following equation:

$$r_i = \rho\sin(\varphi_i). \tag{30}$$

The integral transform involved in Eqs. (28) and (29) is

$$\begin{cases} U_1 = r_{n-1}\rho\sin(\varphi_1), \\ U_2 = r_{n-2}\rho\sin(\varphi_1)\cos(\varphi_2), \\ \quad\vdots \\ U_{n-2} = r_2\rho\sin(\varphi_1)\cdots\sin(\varphi_{n-3})\cos(\varphi_{n-2}), \\ U_{n-1} = r_1\rho\sin(\varphi_1)\cdots\sin(\varphi_{n-3})\sin(\varphi_{n-2}). \end{cases} \tag{31}$$

Therefore, the simplified failure probability formula is derived from substituting Eqs. (25), (28) and (29) into Eq. (23), respectively, as

$$P_{\mathrm{f}} = (2\pi)^{-\frac{n}{2}} \int_{\beta}^{+\infty} S \cdot \exp\left(-\frac{\rho^2}{2}\right) \mathrm{d}\rho. \tag{32}$$

3 Illustrative Examples

In this section, three examples are selected to compare the proposed method with the reliability analysis results of FORM, SORM, SORM-Kriging (SORM combined with Kriging model), and MCS to verify its validity and feasibility. The failure probability obtained by the other reliability methods is $P_{\mathrm{f,R}}$, and the failure probability obtained by the MCS method $P_{\mathrm{f,MCS}}$ with a sample size of 5×10^7 is considered as the reference. Then the accuracy can be expressed as the relative error ε:

$$\varepsilon = \frac{P_{\mathrm{f,MCS}} - P_{\mathrm{f,R}}}{P_{\mathrm{f,MCS}}} \times 100\%. \tag{33}$$

In addition, to evaluate the computational efficiency, assuming that I is the number of iterations of the HLRF algorithm, k is the number of iterations of the

HLRF-BFGS algorithm and n is the dimension of the LSF. Then, the formulas for the number of function evaluations E, specifically E_{FORM} for FORM, E_{SORM} for SORM and E_{TS} for the method of this study, are shown as

$$E_{\mathrm{FORM}} = I(n+1), \tag{34}$$

$$E_{\mathrm{SORM}} = n(n+1)/2 + I(n+1), \tag{35}$$

$$E_{\mathrm{TS}} = k(n+1) + 2n. \tag{36}$$

3.1 Example 1: four-dimensional problem

Example 1 addresses a four-dimensional problem characterized by a high degree of nonlinearity, with the LSF provided as

$$\begin{aligned} g(X_1, X_2, X_3, X_4) = {} & 1\,100 + 71.7X_1^4 - 61.1X_2^4 + 1.17X_1^2 + \\ & 1.57X_2^2 + 3.33X_3^2 + 1\,339X_4^2 - 1.15X_1X_2 + \\ & 1.35X_2X_3 - 14.9X_1X_3 + 558X_1X_2 - 5.34X_1 - \\ & 70.5X_2 - 226X_3 + 998X_4. \end{aligned} \tag{37}$$

Equation (37) involves four independent random variables, X_1, X_2, X_3 and X_4. Their parameter information is summarized in Table 1.

Table 1 Parameter information of random variables for Example 1

Random variable	Distribution	Mean	Standard deviation
X_1	Gumbel	3.0	1.0
X_2	Normal	25.0	5.0
X_3	Normal	0.4	0.4
X_4	Lognormal	0.1	0.1

By the method proposed in this study, the coordinates of the MPP of the LSF in U-space [0.113 4, 0.165 2, 0.132 4, 1.334 8] are determined. The curvature information is obtained by approximating the Hessian matrix using the Kriging model, yielding the parabolic coefficients [0.262 5, 0.455 1, −0.075 1]. Then, the failure probability is computed by using the hyperspherical cap area integral method and compared with the results of the FORM, SORM, SORM-Kriging and MCS. The comparison results are presented in Table 2.

Table 2 Reliability analysis results for Example 1

Method	β	P_{f}	$\varepsilon/\%$	E
FORM	1.370 8	$8.522\,1\times10^{-2}$	60.73	250
SORM	1.652 2	$4.925\,2\times10^{-2}$	7.11	260
SORM-Kriging	1.541 6	$6.158\,1\times10^{-2}$	16.14	258
This study	1.607 1	$5.401\,6\times10^{-2}$	1.88	198
MCS	1.616 2	$5.302\,1\times10^{-2}$	—	5×10^{7}

By analyzing the results in Table 2, it is evident that FORM, by neglecting curvature effects, approximates the LSF as linear, leading to substantial errors. Although SORM provides improved accuracy over FORM, it is less efficient. In contrast, the proposed method in this study, which combines the BFGS algorithm, achieves a number of functional evaluations of only 198 and the relative error is just 1.88%. Consequently, this method demonstrates higher efficiency and accuracy.

3.2 Example 2: reliability analysis of cantilever tube structure

Figure 2 illustrates the forces acting on the cantilever tube. F_1 and F_2 are forces within the xy-plane, torsion T acts within the y-plane, and an axial force W is applied in the x-direction. The maximum stress $\sigma_{\max}$ occurs at point A, which is located at a distance of L_2. D is the diameter of the cantilever tube, and t_1 is the wall thickness of the cantilever tube. The failure criterion is based on $\sigma_{\max}$ exceeding the material yield strength S_{s}. Consequently, the LSF is determined as

$$g(S_{\mathrm{s}}, D, L_2, t_1, F_1, F_2, W, T) = S_{\mathrm{s}} - \sigma_{\max}, \tag{38}$$

$$\sigma_{\max} = \sqrt{\sigma_x^2 + 3\tau_{xz}^2}, \tag{39}$$

where σ_x is the normal stress; τ_{xz} is the torsional stress. σ_x and τ_{xz} can be calculated respectively as

$$\sigma_x = \frac{P + F_1\sin\varphi_1 + F_2\sin\varphi_2}{V} + \frac{(F_1L_1\cos\varphi_1 + F_2L_2\cos\varphi_2)C}{Z}, \tag{40}$$

$$\tau_{xz} = TD/(2J), \tag{41}$$

where

$$V = \pi[D^2 - (D-2t_1)^2]/4, \tag{42}$$

$$Z = \pi[D^4 - (D-4t_1)^4]/64, \tag{43}$$

$$J = 2Z, \tag{44}$$

$$C = D/2. \tag{45}$$

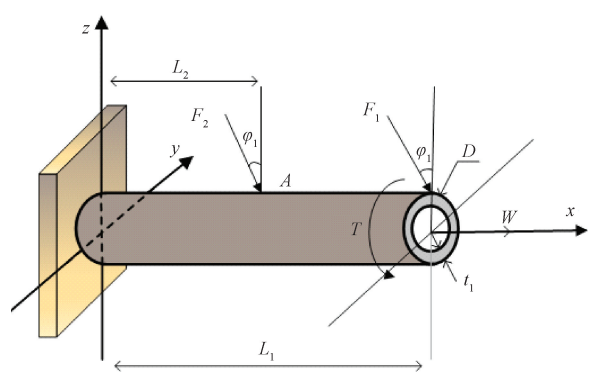

Fig. 2 Structure of a cantilever tube

Assume that $\varphi_1 = 10°$, $\varphi_2 = 15°$ and $L_1 = 200$ mm. All eight random variables of this LSF obey a lognormal distribution, and the detailed information is shown in Table 3.

Table 3 Parameter information of random variables for Example 2

Random variable	Unit	Description	Distribution	Mean	Standard deviation
S_s	MPa	Yield strength of material	Lognormal	350.00	35.00
D	mm	Diameter of cantilever tube	Lognormal	40.00	0.40
L_2	mm	Distance to point A	Lognormal	80.00	4.00
t_1	mm	Wall thickness of cantilever tube	Lognormal	4.00	0.04
F_1	kN	Force at L_1	Lognormal	4.00	0.40
F_2	kN	Force at L_2	Lognormal	4.00	0.40
W	kN	Axial force	Lognormal	12.00	1.20
T	kN·m	Torsion	Lognormal	0.12	0.08

The MPP is located at [−2.504 2, −0.534 3, 0.313 4, −0.147 2, 2.101 6, 0.585 2, −0.237 1, 0.165 8], and the approximate parabolic coefficient is [−0.065 1, −0.065 8, 0.007 8, −0.005 3, −0.000 6, −0.001 3, −0.001 8]. The computational data is shown in Table 4. Although FORM evaluates the function fewer times, it exhibits a substantial error. In contrast, the method proposed in this study demonstrates superior efficiency and accuracy compared to SORM. Thus, the feasibility of the proposed method is further validated through this complex engineering structure example.

Table 4 Reliability analysis results for Example 2

Method	β	P_f	ε/%	E
FORM	3.400 9	$3.358\ 5 \times 10^{-4}$	33.37	252
SORM	3.361 5	$3.875\ 9 \times 10^{-4}$	23.11	284
SORM-Kriging	3.370 1	$3.756\ 8 \times 10^{-4}$	25.47	272
This study	3.280 0	$5.189\ 7 \times 10^{-4}$	2.96	259
MCS	3.288 3	$5.040\ 6 \times 10^{-4}$	—	5×10^7

3.3 Example 3: reliability analysis of truss structure

Figure 3 shows a ten-bar truss structure with external loads of 4.448×10^6 N applied at nodes 5 and 6. The maximum allowable displacement at node 6 is $u_{max} = 50.8$ cm, exceeding which the structure fails. The implicit limit state function involved in this example is

$$g(\boldsymbol{X}) = u_{max} - u_3(X_1, X_2, \cdots, X_{10}), \quad (46)$$

where $(X_1, X_2, \cdots, X_{10})$ have a mean of 1 and a standard deviation of 2, and both follow a standard normal distribution.

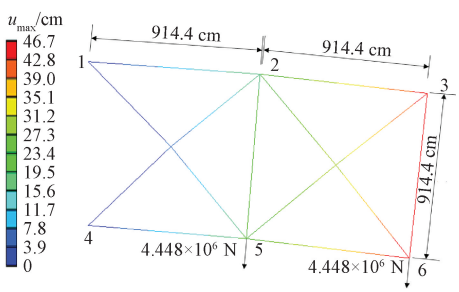

Fig. 3 Structure of a ten-bar truss by finite element analysis

Finite element analysis was used to calculate $u_3(X_1, \cdots, X_{10})$. Then, the Kriging model was constructed by using the Latin hypercube sampling method generated from 1 024 sample points. In this example, the MPP can be obtained as [1.959 7, 2.496 4, 1.790 1, 2.438 2, 2.524 6, 2.454 7, 2.296 2, 2.297 3, 2.390 8, 2.448 3] and the approximate parabolic coefficient is [−0.143 4, 0.086 2, −0.067 1, 0.061 5, −0.012 4, −0.008 5, 0.005 3, 0.001 3]. The computational results for different reliability analysis methods are shown in Table 5. It can be observed that the method proposed in this study still maintains high accuracy and efficiency for the implicit limit state function.

Table 5 Reliability analysis results for Example 3

Method	β	P_f	ε/%	E
FORM	1.896 8	$2.892\ 6 \times 10^{-2}$	7.69	6 622
SORM	1.741 0	$4.084\ 1 \times 10^{-2}$	30.34	6 677
SORM-Kriging	1.748 5	$4.018\ 9 \times 10^{-2}$	28.26	6 642
This study	1.861 5	$3.220\ 8 \times 10^{-2}$	2.79	5 520
MCS	3.288 3	$3.133\ 4 \times 10^{-2}$	—	5×10^7

4 Conclusions

1) This study enhances the convergence and efficiency of the iterative process by utilizing the HLRF-BFGS algorithm to accurately identify the design point. Furthermore, the Hessian matrix is approximated by using the Kriging model, which effectively reduces the computational workload.

2) The principal curvature of the approximated parabolic function is derived from the Hessian matrix. Additionally, employing the hyperspherical cap area integral method improves the precision of failure probability calculations.

3) Validation through three examples shows that the proposed method offers enhanced computational accuracy and efficiency compared to existing methods.

4) As the accuracy of the Kriging model is closely tied to the accurate solution of the Hessian matrix, future research should focus on improving the precision of the Kriging model to further enhance the reliability and

effectiveness of the proposed method.

References

[1] CHEN Z Z, WU Z H, LI X K, et al. An accuracy analysis method for first-order reliability method [J]. *Proceedings of the Institution of Mechanical Engineers, Part C: Journal of Mechanical Engineering Science*, 2019, 233(12): 4319-4327.

[2] YANG M D, ZHANG D Q, HAN X. New efficient and robust method for structural reliability analysis and its application in reliability-based design optimization [J]. *Computer Methods in Applied Mechanics and Engineering*, 2020, 366: 113018.

[3] ZHONG X, YANG R Q, ZHOU B. Accuracy analysis of assembly success rate with Monte Carlo simulations [J]. *Journal of Donghua University (English Edition)*, 2003, 20(4): 128-131.

[4] AU S K, BECK J L. Estimation of small failure probabilities in high dimensions by subset simulation [J]. *Probabilistic Engineering Mechanics*, 2001, 16(4): 263-277.

[5] GROOTEMAN F. An adaptive directional importance sampling method for structural reliability [J]. *Probabilistic Engineering Mechanics*, 2011, 26(2): 134-141.

[6] XIAO N C, ZUO M J, ZHOU C N. A new adaptive sequential sampling method to construct surrogate models for efficient reliability analysis [J]. *Reliability Engineering & System Safety*, 2018, 169: 330-338.

[7] XIAO N C, YUAN K, ZHOU C N. Adaptive Kriging-based efficient reliability method for structural systems with multiple failure modes and mixed variables [J]. *Computer Methods in Applied Mechanics and Engineering*, 2020, 359: 112649.

[8] GAO J, LUO Z, LI H, et al. Topology optimization for multiscale design of porous composites with multi-domain microstructures [J]. *Computer Methods in Applied Mechanics and Engineering*, 2019, 344: 451-476.

[9] HASOFER A M, LIND N C. Exact and invariant second-moment code format [J]. *Journal of the Engineering Mechanics Division*, 1974, 100(1): 111-121.

[10] RACKWITZ R, FLESSLER B. Structural reliability under combined random load sequences [J]. *Computers & Structures*, 1978, 9(5): 489-494.

[11] KESHTEGAR B, MENG Z. A hybrid relaxed first-order reliability method for efficient structural reliability analysis [J]. *Structural Safety*, 2017, 66: 84-93.

[12] MENG Z, LI G, WANG B P, et al. A hybrid chaos control approach of the performance measure functions for reliability-based design optimization [J]. *Computers & Structures*, 2015, 146: 32-43.

[13] PERIÇARO G A, SANTOS S R, RIBEIRO A A, et al. HLRF-BFGS optimization algorithm for structural reliability [J]. *Applied Mathematical Modelling*, 2015, 39(7): 2025-2035.

[14] ZHANG J F, DU X P. A second-order reliability method with first-order efficiency [J]. *Journal of Mechanical Design*, 2010, 132(10): 101006.

[15] ZENG P, CHEN Y, LI T B. System reliability of geotechnical problems using quasi-Newton approximation-based sorm [J]. *Chinese Journal of Rock Mechanics and Engineering*, 2018, 37(3): 726-733. (in Chinese)

[16] CHEN Z Z, HUANG D Y, TIAN J, et al. Structural reliability analysis method based on second order parabolic approximation [J]. *Journal of Engineering Design*, 2024, 31(1): 50-58. (in Chinese)

[17] CHEN Z Z, MU H X, LI X K, et al. A hyperspherical cap area integral method for reliability analysis [J]. *Computers & Structures*, 2024, 298: 107372.

[18] CHEN Z Z. Research on accurate decoupling and efficient sampling technology in reliability-based design optimization [D]. Wuhan: Huazhong University of Science and Technology, 2013. (in Chinese)

[19] Rosenblatt M. Remarks on a multivariate transformation [J]. *Annals of Mathematical Statistics*, 1952, 23(3): 470-472.

[20] KARL B. Asymptotic approximations for multinormal integrals [J]. *Journal of Engineering Mechanics*, 1984, 110(3): 357-366.

[21] CAI G Q, ELISHAKOFF I. Refined second-order reliability analysis [J]. *Structural Safety*, 1994, 14(4): 267-276.

基于 Kriging 模型和球冠区域积分的结构可靠性分析方法

张吉祥[1]，陈振中[1*]，陈　革[1*]，李晓科[2]，赵鹏程[3]，潘强华[4]

1. 东华大学 机械工程学院，上海 201620
2. 郑州轻工业大学 机电工程学院，河南 郑州 450002
3. 上海科创职业技术学院，上海 201620
4. 中国特种设备检测研究院，北京 100029

摘　要：在结构可靠性分析中，一阶可靠性方法处理非线性问题会产生显著误差，二阶可靠性方法能够提供更高的精度，但额外计算 Hessian 矩阵，会使计算效率降低。此外，当随机变量的维数较高时，二阶可靠性方法受到近似公式的影响也会产生较大的误差。为了解决这些问题，该文提出了一种基于 Kriging 模型和球冠区域积分的结构可靠性分析方法。该方法首先将一阶可靠性方法与拟牛顿算法 BFGS 相结合，利用算法迭代过程中的样本点训练 Kriging 模型，并将 Kriging 模型与梯度信息结合以构建 Hessian 矩阵的近似表示。其次，将失效面近似为旋转抛物面，并使用球冠区域代替复杂曲面。在 n 维情况下，通过结合超球冠面积表达式和积分方法来求解失效概率。最后，用三个算例验证了该方法，相比于传统方法，该方法在计算精度和效率上均有所提升。

关键词：结构可靠性分析；拟牛顿算法；Kriging 模型；球冠区域积分